Simultaneous wavelength translation and amplitude modulation of single photons from a quantum dot

Matthew T. Rakher,[1,*] Lijun Ma,[2] Marcelo Davanço,[1,3]

Oliver Slattery,[2] Xiao Tang,[2] and Kartik Srinivasan[1]

[1]*Center for Nanoscale Science and Technology,*

National Institute of Standards and Technology, Gaithersburg, MD 20899, USA

[2]*Information Technology Laboratory,*

National Institute of Standards and Technology, Gaithersburg, MD 20899, USA

[3]*Maryland NanoCenter, University of Maryland, College Park, MD 20742, USA*

(Dated: August 16, 2011)

Abstract

Hybrid quantum information devices that combine disparate physical systems interacting through photons offer the promise of combining low-loss telecommunications wavelength transmission with high fidelity visible wavelength storage and manipulation. The realization of such systems requires control over the waveform of single photons to achieve spectral and temporal matching. Here, we experimentally demonstrate the simultaneous wavelength conversion and temporal shaping of single photons generated by a quantum dot emitting near 1300 nm with an exponentially-decaying waveform (lifetime $\approx$1.5 ns). Quasi-phase-matched sum-frequency generation with a pulsed 1550 nm laser creates single photons at 710 nm with a controlled amplitude modulation at 350 ps timescales.

The integration of disparate quantum systems is an ongoing effort in the development of distributed quantum networks [1]. Two challenges in hybrid schemes which use photons for coupling include the differences in transition frequencies and linewidths among the component systems. Previous experiments that used non-linear optical media to translate (or transduce) photons from one wavelength to another while preserving quantum-mechanical properties [2, 3] provide a means to overcome the first impediment. The second constraint has been addressed through single photon waveform manipulation using direct electro-optic modulation [4], Λ-type cavity-QED [5] and atomic ensemble systems [6], and conditional, non-local operations in spontaneous parametric downversion [7]. Here, we use pulsed frequency upconversion to simultaneously change the frequency and temporal amplitude profile of single photons produced by a semiconductor quantum dot (QD). Triggered single photons that have an exponentially decaying temporal profile with a time constant of 1.5 ns and a wavelength of 1300 nm are converted to photons that have a Gaussian temporal profile with a controllable full-width at half-maximum (FWHM) as narrow as 350 ps ± 16 ps and a wavelength of 710 nm. The use of a high conversion efficiency nonlinear waveguide and low-loss fiber optics results in a 16 % overall efficiency in producing such frequency converted, amplitude-modulated photons. This simultaneous combination of wavepacket manipulation and quantum frequency conversion may be valuable in integrating telecommunications-band semiconductor QDs with broadband visible wavelength quantum memories [8] as part of a distributed quantum network and for the creation of ultra-high bandwidth, indistinguishable photons from disparate quantum emitters.

Single epitaxially-grown semiconductor QDs are promising stable, bright, and scalable on-demand sources of single photons [9], with improvements in photon extraction efficiency [10], suppression of multi-photon events [10, 11], and photon indistinguishability [11, 12] indicative of their potential for high performance in quantum information applications. On the other hand, these developments have taken place using QDs in the InGaAs/GaAs material system which constrains their emission energies and temporal control of the photon wavepacket shape remains a challenge in these systems. Efforts have been made to develop QDs in other material systems [13], but this work has not resulted in the same quality of single photons as those produced in InGaAs/GaAs. In addition, despite recent progress [14] access to three-level Raman transitions in which the temporal shape is determined by the pump mode profile, a staple of trapped atom and ion systems [5, 15] is typically not available.
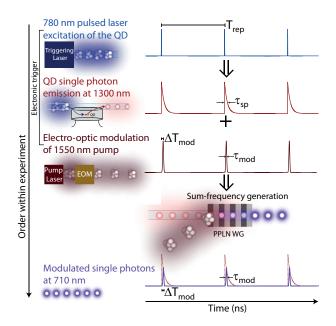
2

FIG. 1. Schematic of the experiment for simultaneous wavelength translation and amplitude modulation of single photons from a quantum dot.

Instead, most QDs are two-level systems in which the emitted photons have an exponentially decaying temporal profile, and temporal shaping must occur after photon generation. As we describe below, the method used in this work produces wavelength-translated, single photon wavepackets with a temporal profile inherited from the classical pump beam used in the pulsed frequency upconversion process. Though this technique is not lossless, it can still be quite efficient, is flexible, straightforward to use on existing devices, and operates on the nanosecond timescales requisite for QD experiments and for which classical coherent pulse shaping techniques [16] are difficult to implement. In comparison to direct amplitude modulation of single photon wavepackets [4], the technique presented here has lower loss, can operate on much faster timescales using existing mode-locked laser technologies, and importantly, simultaneously changes the wavelength of the photons. This is necessary for integration with visible wavelength quantum systems and provides a method to overcome spectral and temporal distinguishability of disparate quantum sources. As shown below, fast upconversion can also be used to achieve efficient, temporally-resolved detection at the ps level, beyond the capabilities of existing photon counters. In addition, recent theoretical work has shown that a similar nonlinear mixing approach can be used for lossless pulse shaping and compression of single photons from a two-level quantum emitter [17].

We generated single photons at 1.3 μm from a single InAs QD embedded in a GaAs mesa, as described in detail in the supplemental material. The QD sample is cooled to a temperature of $\approx$7 K and an optical fiber taper waveguide (FTW) is used to both excite the sample with a repetitively pulsed (50 MHz) laser and collect its photoluminescence (PL) as depicted in Fig. 1. The PL is directed either into a grating spectrometer for characterization or into the pulsed upconversion setup for simultaneous wavelength translation and amplitude modulation. The PL spectrum from a single QD measured by the spectrometer is shown in Fig. 2(a). It displays two sharp peaks corresponding to two excitonic charge configurations, X^+ near 1296 nm, and X^0 near 1297 nm. Photons emitted at the X^0 transition wavelength will be used for the experiments described hereafter.

PL from the X^0 transition is directed into an upconversion setup where it is combined with a strong 1550 nm pulse in a periodically-poled LiNbO$_3$ (PPLN) waveguide (see supplemental material for details). A simplified schematic of the experimental timing sequence is shown in Fig. 1. The pump pulse is created by gating the output of a tunable laser with an electro-optic modulator (EOM). An electrical pulse generator drives the EOM synchronously with the 780 nm QD excitation laser, but at half the repetition rate (25 MHz), using a trigger signal from the delay generator. These instruments combine to generate electrical pulses with controllable FWHM (τ_{mod}) and delay (ΔT_{mod}) as shown in Fig. 2(a), and the resulting optical pulses have an extinction ratio > 20 dB. The modulated 1550 nm pump signal is amplified to produce a peak power of 80 mW entering the PPLN waveguide where it interacts with a 1300 nm QD single photon to create a single photon at the sum-frequency near 710 nm. This $\chi^{(2)}$ process is made efficient through quasi-phase-matching by periodic poling [18] as well as the tight optical confinement of the waveguide [19]. Previous measurements using a continuous-wave (CW) pump in the same setup demonstrated single-photon conversion efficiencies of at least $\gtrsim$ 75 % [3], and others have measured efficiencies near unity with attenuated laser pulses [20, 21]. Light exiting the PPLN is spectrally filtered to isolate the 710 nm photons, which are detected by Si single photon counting avalanche detectors (SPADs) for excited state lifetime and second-order correlation measurement ($g^{(2)}(\tau)$).

First, we compare the measured $g^{(2)}(\tau)$ for photons that are upconverted using a 1550 nm CW pump (Fig. 2(b)) and 500 ps pulses (Fig. 2(c)) with the same peak power of 80 mW. Both are antibunched with $g^{(2)}(0) < 0.5$, showing that the signal is dominantly composed of single photons in both cases. However, pulsed pumping reduces events that are uncorrelated
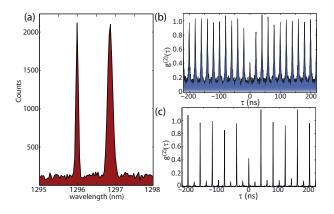
4

FIG. 2. (a) PL spectrum of a single QD after 60 s integration showing two excitonic transitions, X^+ (1296 nm) and X^0 (1297 nm). (b-c) Second-order intensity correlation, $g^{(2)}(\tau)$, of single photons upconverted with a CW pump, where $g^2(0) = 0.41 \pm 0.02$ (c) and a pulsed pump with τ_{mod}=500 ps, where $g^2(0) = 0.45 \pm 0.03$ (d) for an integration time of 7200 s.

in time with the QD single photons and contribute a constant background. This unwanted background results from upconversion of anti-Stokes Raman photons from the strong (CW) 1550 nm beam [20], and is seen in Fig. 2(b) but not in Fig. 2(c). For understanding the origin of the non-zero $g^{(2)}(0)$ value, the background is helpful in distinguishing the fraction due to anti-Stokes Raman photons from that due to upconversion of multi-photon emission from the QD sample [3]. For practical implementation, however, it adds a constant level to the communications channel, and as shown in Fig. 2(c), pulsed upconversion removes this noise without gating of the detector. Ideally, Fig. 2(c) would only show peaks spaced by 40 ns, due to the 25 MHz repetition rate of the EOM. In practice, the small peaks spaced 20 ns from the large peaks are due to imperfect extinction of the EOM and pulse generator signal, resulting in upconversion of QD photons when the EOM is nominally off.

Next, we perform time-resolved measurements of the upconverted 710 nm photons. In recent work [3] using a CW 1550 nm pump beam, the temporal amplitude profile of the upconverted 710 nm photon exactly matched that of the original 1300 nm photon, and was used to measure the QD lifetime with dramatically better SNR than with a telecommunications SPAD. Here, the pulsed 1550 nm pump not only upconverts the QD photon to 710 nm, but also modulates its temporal amplitude profile because τ_{mod} is less than the lifetime of the QD transition (≈ 1.5 ns). Figure 3(a) displays the temporal amplitude profile of 710 nm single photons generated using a 1550 nm pulse with $\tau_{mod} = 260$ ps (maroon), along with
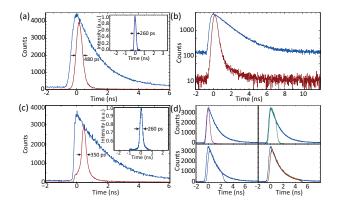
FIG. 3. (a,b) Temporal profile of the upconverted photons using a CW (blue) and τ_{mod} =260 ps pulsed (maroon) 1550 nm pump on linear (a) and log (b) scales. Inset: 1550 nm pump pulse measured by the optical communications analyzer. (c) Same as (a) but using a reduced timing jitter SPAD. (d) Temporal profile of upconverted photons using $\tau_{mod} = \{0.5, 1.25, 2.5, 5.1\}$ ns along with a CW pump. All measurements are taken with 1200 s integration.

that of single photons generated with a CW pump (blue) for comparison. The measured 480 ps $\pm$ 16 ps FWHM of the upconverted photon is limited by the $\approx$350 ps timing jitter of the Si SPAD and its uncertainty is given by the timebase of the photon counting board. The same plot is reproduced in Fig. 3(b) on a log scale, with an apparent increase in the dynamic range due to the removal of CW anti-Stokes Raman photons. This same measurement was performed using a SPAD with a reduced timing jitter ($\approx$ 50 ps), and the resulting data is shown in Fig. 3(c) corresponding to a FWHM of 350 ps $\pm$ 16 ps. Here, the resulting FWHM is not limited by the detector timing jitter but by an effective broadening of the pump pulse in the frequency conversion process (see supplemental material for details). Even so, taken together with the commercial availability of 40 GHz EOMs and drivers for 1550 nm lasers, these results demonstrate a first step towards the creation of quantum light sources that are modulated to operate near the capacity of telecommunications channels [17]. To show the versatility of the setup, Fig. 3(d) shows the temporal profile of QD single photons after up-conversion using pump pulse widths of $\tau_{mod} = 500$ ps, 1.25 ns, 2.5 ns, and 5.1 ns along with a CW pump for comparison. By simply adjusting the pulse generator that drives the EOM, one can create single photons of arbitrary width and shape (see supplemental material).

In addition to changing τ_{mod}, the delay between the arrival of the QD single photon and pump pulse, ΔT_{mod}, can also be varied (Fig. 2(a)). Figure 4(a)-(b) show the result of such a

measurement in linear (a) and log (b) scale for $\Delta T_{mod} = \{0.0, 0.5, 1.0, 1.5, 2.0, 2.5, 3.0, 3.35\}$ ns under pulsed pumping with $\tau_{mod} = 260$ ps. The inset of (a) shows a similar measurement using the reduced timing jitter SPAD. The peaks heights nicely follow the decay curve of the CW profile, shown in blue for comparison. This measurement suggests that pulsed frequency upconversion could be used for achieving high timing resolution in experiments on single quantum emitters. These time-correlated single photon counting experiments are currently limited by the timing jitter of the SPAD, which is typically > 50 ps. The time-domain sampling enabled by pulsed upconversion [22] provides a timing resolution set by τ_{mod}, which is limited by the quasi-phase matching spectral bandwidth of the non-linear material. For the PPLN waveguide used here, the bandwidth (≈ 0.35 nm) corresponds to a minimum $\tau_{mod} \approx 10$ ps, while sub-ps timing resolution should be available in broader bandwidth systems [23]. Sub-ps 1550 nm pulses can be generated by mode-locked fiber lasers, and if applied as in Fig. 4(a)-(b), could trace out emission dynamics with a timing resolution 1-2 orders of magnitude better than the typical timing jitter of a SPAD, allowing, for example, measurement of beat phenomena within the QD [24] or time-domain observation of vacuum Rabi oscillations in cavity quantum electrodynamics [25].
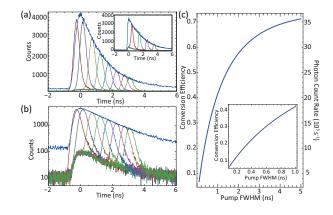

FIG. 4. (a,b) Temporal profile of the upconverted photons using a CW (blue) and $\tau_{mod} =260$ ps pulsed (various colors) 1550 nm pump on linear (a) and log (b) scales for delays $\Delta T_{mod} = \{0.0, 0.5, 1.0, 1.5, 2.0, 2.5, 3.0, 3.35\}$ ns. Inset: Similar measurement as (a), but measured with reduced timing jitter SPAD. All measurements are taken with 1200 s integration. (c) Net conversion efficiency and photon count rate as a function of the pump pulse FWHM, τ_{mod}. Inset: Focus on sub-ns regime.

The data from Figs. 2 and 3 indicate that while the quantum nature of the photon has

7

been inherited from the QD emission near 1300 nm, its temporal profile has been inherited from the strong pump pulse near 1550 nm. This is a direct consequence of the nonlinear nature of the upconversion process. However, because QD-generated single photons have a coherence time that is typically less than twice the lifetime, they are not perfectly indistinguishable [12]. This arises due to interaction of the confined carriers in the QD with the surrounding crystal and, for the type of QD considered here, yields a coherence time of ≈ 280 ps [25] and an indistinguishability of ≈ 10 %. For our experiments, this means that each photon is not modulated in the same way and the resulting histograms are ensemble averages. Nonetheless, the experiments would proceed in the exact same manner for more ideal photons, such as those produced with a ns coherence time through near-resonant excitation [11]. In fact, simultaneous frequency translation and amplitude modulation can be used to generate indistinguishable single photons from non-identical QDs [26]. Frequency translation can move each single photon to the same wavelength while amplitude modulation can be used to select the coherent part of the wave-packet. Since the quasi-phase matching of the PPLN can be tuned by temperature, this offers the ability to create indistinguishable single photons from QDs spectrally separated by the entire inhomogeneous linewidth of the QD distribution (which is usually tens of nanometers) without the need for electrical gates or modification of the sample.

The single photon manipulation demonstrated here is essentially a combination of quantum frequency conversion and amplitude modulation. Coherent pulse-shaping techniques [16], which have been used with entangled photon pairs [27], are currently quite difficult to directly apply to QD single photons due to their narrow spectral bandwidth compared to photons produced by parametric downconversion, for example. Furthermore, recent work [17] has suggested that a combination of frequency upconversion using a spectrally tailored 1550 nm pump beam and spectral phase correction may be an approach to lossless shaping of QD single photons. Our work, utilizing a similar sum frequency generation approach, represents a step towards such a goal. Though our approach is not lossless, broadband insertion loss (usually > 3 dB) is avoided in comparison to direct amplitude modulation of the single photon state because the modulation in nonlinear mixing approaches such as ours and that of Ref. [17] is performed on the classical pump beam. Nonetheless, the fact that the pump pulse is temporally shorter than the single photon wave-packet introduces extra loss. A full derivation of this loss is included in the supplemental material,

but the result is shown in Fig. 4(c) which plots the net conversion efficiency as a function of the pump pulse FWHM, τ_{mod}, from 100 ps to 5 ns (inset displays sub-ns regime). The efficiency asymptotically approaches 75 %, the measured conversion efficiency with a CW pump, and ranges from 16 % for $\tau_{mod} = 260$ ps to 71 % for $\tau_{mod} = 5$ ns. For our FTW-based PL collection with 0.1 % collection efficiency and 50 MHz excitation rate, this translates to a single photon count rate of 8000 s^{-1} to 36000 s^{-1} as shown on the right axis in Fig. 4(c). Using more advanced techniques that have demonstrated >10 % collection efficiency [10], the overall production rate of frequency translated, temporally modulated single photons can easily reach 10^6 s^{-1}.

In summary, we have demonstrated quantum frequency upconversion of QD-generated single photons with a pulsed pump. While the upconverted light is still dominantly composed of single photons, its temporal amplitude profile is changed to match that of the classical pump. We measure Gaussian-shaped single photon profiles with FWHMs as narrow as 350 ps ± 16 ps, limited by the electrical pulse generator. Such methods may prove valuable for integrating disparate quantum systems, creating ultra-high bandwidth single photon sources, and for achieving high resolution in time-resolved experiments of single quantum systems.

----

* matthew.rakher@gmail.com; Current Address: Departement Physik, Universität Basel, Klingelbergstrasse 82, CH-4056 Basel, Switzerland

[1] H. J. Kimble, Nature (London) **453**, 1023 (2008).

[2] J. M. Huang and P. Kumar, Phys. Rev. Lett. **68**, 2153 (1992); S. Tanzilli, W. Tittel, M. Halder, O. Alibart, P. Baldi, N. Gisin, and H. Zbinden, Nature **437**, 116 (2005); H. J. McGuinness, M. G. Raymer, C. J. McKinstrie, and S. Radic, Phys. Rev. Lett. **105**, 093604 (2010).

[3] M. T. Rakher, L. Ma, O. Slattery, X. Tang, and K. Srinivasan, Nature Photonics **4**, 786 (2010).

[4] P. Kolchin, C. Belthangady, S. Du, G. Y. Yin, and S. E. Harris, Phys. Rev. Lett. **101**, 103601 (2008); H. P. Specht, J. Bochmann, M. Mücke, B. Weber, E. Figueroa, D. L. Moehring, and G. Rempe, Nature Photonics **3**, 469 (2009); M. T. Rakher and K. Srinivasan, Appl. Phys. Lett. **98**, 211103 (2011).

[5] J. McKeever, A. Boca, A. D. Boozer, R. Miller, J. R. Buck, A. Kuzmich, and H. J. Kimble, Science **303**, 1992 (2004); M. Keller, B. Lange, K. Hayaska, W. Lange, and H. Walther, Nature **431**, 1075 (2004).

[6] M. D. Eisaman, L. Childress, A. André, F. Massou, A. S. Zibrov, and M. D. Lukin, Phys. Rev. Lett. **93**, 233602 (2004); J. F. Chen, S. Zhang, H. Yan, M. M. T. Loy, G. K. L. Wong, and S. Du, *ibid.* **104**, 183604 (2010).

[7] S.-Y. Baek, O. Kwon, and Y.-H. Kim, Phys. Rev. A **77**, 013829 (2008).

[8] K. F. Reim, J. Nunn, V. O. Lorenz, B. J. Sussman, K. C. Lee, N. K. Langford, D. Jaksch, and I. A. Walmsley, Nature Photonics **4**, 218 (2010); E. Saglamyurek, N. Sinclair, J. Jin, J. A. Slater, D. Oblak, F. Bussières, M. George, R. Ricken, W. Sohler, and W. Tittel, Nature (London) **469**, 512 (2011).

[9] A. J. Shields, Nature Photonics **1**, 215 (2007).

[10] S. Strauf, N. G. Stoltz, M. T. Rakher, L. A. Coldren, P. M. Petroff, and D. Bouwmeester, Nature Photonics **1**, 704 (2007); J. Claudon, J. Bleuse, N. S. Malik, M. Bazin, P. Jaffrennou, N. Gregersen, C. Sauvan, P. Lalanne, and J. Gérard, *ibid.* **4**, 174 (2010).

[11] S. Ates, S. M. Ulrich, S. Reitzenstein, A. Löffler, A. Forchel, and P. Michler, Phys. Rev. Lett. **103**, 167402 (2009).

[12] C. Santori, D. Fattal, J. Vuckovic, G. Solomon, and Y. Yamamoto, Nature **419**, 594 (2002).

[13] N. Akopian, U. Perinetti, L. Wang, A. Rastelli, O. G. Schmidt, and V. Zwiller, Appl. Phys. Lett. **97**, 082103 (2010); N. Akopian, L. Wang, A. Rastelli, O. G. Schmidt, and V. Zwiller, Nature Photonics **5**, 230 (2011).

[14] G. Fernandez, T. Volz, R. Desbuquois, A. Badolato, and A. Imamoglu, Phys. Rev. Lett. **103**, 087406 (2009).

[15] G. S. Vasilev, D. Ljunggren, and A. Kuhn, New Journal of Physics **12**, 063024 (2010).

[16] A. M. Weiner, Review of Scientific Instruments **71**, 1929 (2000).

[17] D. Kielpinski, J. F. Corney, and H. M. Wiseman, Phys. Rev. Lett. **106**, 130501 (2011).

[18] M. M. Fejer, G. A. Magel, D. H. Jundt, and R. L. Byer, IEEE J. Quan. Elec. **28**, 2631 (1992).

[19] L. Chanvillard, P. Aschiéri, P. Baldi, D. B. Ostrowsky, M. de Micheli, L. Huang, and D. J. Bamford, Appl. Phys. Lett. **76**, 1089 (2000).

[20] C. Langrock, E. Diamanti, R. Roussev, Y. Yamamoto, M. Fejer, and H. Takesue, Opt. Lett. **30**, 1725 (2005).

[21] A. Vandevender and P. Kwiat, J. Mod. Opt. **51**, 1433 (2004); M. Albota and F. Wong, Opt. Lett. **29**, 1449 (2004); H. Xu, L. Ma, A. Mink, B. Hershman, and X. Tang, Opt. Express **15**, 7247 (2007).

[22] J. Shah, IEEE J. Quan. Elec. **24**, 276 (1988); L. Ma, J. C. Bienfang, O. Slattery, and X. Tang, Opt. Express **19**, 5470 (2011).

[23] O. Kuzucu, F. N. C. Wong, S. Kurimura, and S. Tovstonog, Opt. Lett. **33**, 2257 (2008); H. Suchowski, B. D. Bruner, A. Arie, and Y. Silberberg, Opt. Photon. News **21**, 36 (2010).

[24] T. Flissikowski, A. Hundt, M. Lowisch, M. Rabe, and F. Henneberger, Phys. Rev. Lett. **86**, 3172 (2001).

[25] K. Srinivasan, C. P. Michael, R. Perahia, and O. Painter, Phys. Rev. A **78**, 033839 (2008).

[26] R. B. Patel, A. J. Bennett, I. Farrer, C. A. Nicoll, D. A. Ritchie, and A. J. Shields, Nature Photonics **4**, 632 (2010); E. B. Flagg, A. Muller, S. V. Polyakov, A. Ling, A. Migdall, and G. S. Solomon, Phys. Rev. Lett. **104**, 137401 (2010).

[27] A. Pe'er, B. Dayan, A. A. Friesem, and Y. Silberberg, Phys. Rev. Lett. **94**, 073601 (2005).

Simultaneous wavelength translation and amplitude modulation of single photons from a quantum dot: Supporting Material

Matthew T. Rakher,[1, *] Lijun Ma,[2] Marcelo Davanço,[1, 3] Oliver Slattery,[2] Xiao Tang,[2] and Kartik Srinivasan[1]

[1] Center for Nanoscale Science and Technology, National Institute of Standards and Technology, Gaithersburg, MD 20899, USA
[2] Information Technology Laboratory, National Institute of Standards and Technology, Gaithersburg, MD 20899, USA
[3] Maryland NanoCenter, University of Maryland, College Park, MD 20742, USA

EXPERIMENTAL SETUP

We include here a more complete description of the experimental setup discussed in the primary manuscript. A schematic of the experimental apparatus is shown in Fig. 1.
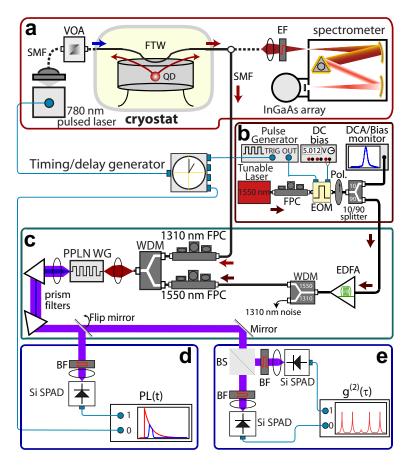

FIG. 1. Experimental setup. (a) Generation of single photons from a QD. (b) 1550 nm tunable pulsed laser source. (c) Pulsed frequency upconversion system. (d) Lifetime and (e) second-order correlation setups. Acronyms: SMF=single mode fiber, VOA=variable optical attenuator, FTW=fiber taper waveguide, QD=quantum dot, EF=edgepass filter, FPC=fiber polarization controller, EOM=electro-optic modulator, EDFA=Erbium-doped fiber amplifier, Pol=polarizer, WDM=wavelength division multiplexer, PPLN WG=periodically-poled lithium niobate waveguide, BF=bandpass filter, BS=beamsplitter, SPAD=single photon counting avalanche photodiode, PL=photoluminescence.

QD Sample Preparation and PL Extraction

InAs quantum dots (QDs) are grown by molecular beam epitaxy in a 256 nm thick device layer. These QDs are made to self-assemble in an InGaAs quantum well (often called DWELL QDs), providing efficient carrier capture [1]. Mesas of 2 μm diameter are etched and physically isolated 1.5 μm above the rest of the sample by a combination of

electron beam lithography, and wet and dry etching [2]. Photoluminescence (PL) is excited and extracted from the sample by a fiber taper waveguide (FTW) as depicted in Fig. 1. The FTW is fabricated by heating and stretching a single mode fiber over a hydrogen flame [3]. The taper is formed adiabatically over a total distance of ≈20 mm and reaches a minimum diameter of ≈1 μm at its center. There, the propagating field can interact with nearby nanophotonic elements through its evanescent tail which extends into free-space. Typical transmission levels through the tapered region are > 95 %. The FTW is brought into contact with the QD-containing mesas by cryogenically compatible nanopositioning stages for extraction stability over the timescales of the measurement. The sample and FTW are contained in a liquid He flow cryostat that reaches a base temperature of ≈7 K. The FTW efficiently excites collects the QD PL into single mode fiber and we estimate for our setup that the FTW collects ≈ 0.1 % of the total QD emission [4].

Pulsed Upconversion Setup

A tunable, external-cavity diode laser near 1550 nm is used to properly achieve quasi-phase matching with the X^0 QD transition in the PPLN waveguide. By tuning the 1550 nm wavelength and monitoring the upconverted count rate near 710 nm, we measure the QD spectrum [5–7], now translated in wavelength, and extract the optimal 1550 nm wavelength. Then, the 1550 nm power is adjusted by changing the current in the EDFA to achieve optimal conversion efficiency, which we have estimated to be $\gtrsim$ 75 % [4]. As depicted in Fig. 1, optical pulses are created by amplitude modulating the CW laser with a fiber-based EOM, which is composed of a micro-fabricated Mach-Zehnder interferometer with a phase modulator. The EOM is driven by a pulse generator and a DC bias. The pulse generator is triggered using a TTL signal from a delay generator, which in turn is triggered by a synchronous signal from the 780 nm pulsed laser that excites the QD. Because of limitations of the delay generator, the pulse generator is triggered at half (25 MHz) the repetition rate of the 780 nm pulsed laser (50 MHz). The output of the EOM is split at a 90:10 beamsplitter, and the 10 % port is used to continuously monitor the pulse with a digital communications analyzer (DCA) so the DC bias is always optimized for minimum/maximum EOM transmission when the pulse generator is in an off state. These instruments combine to create pulses of user-defined width and delay that have an extinction ratio > 20 dB. The 90 % port is directed into the EDFA where the pulse is amplified to achieve a peak power of 85 mW entering the PPLN waveguide, which corresponds to the optimum conversion efficiency [4]. The EDFA output is spectrally filtered with a WDM to extract any 1300 nm noise. The 1550 nm pump pulse is combined with the QD single photons with another WDM after polarization manipulation. This light is coupled out of fiber with a lens and focused into the PPLN waveguide. This waveguide is available commercially and was purchased from HC Photonics [8]. It is 5 cm long and isolated from the environment in a temperature controlled oven at 61.0 °C±0.1 °C. Light exiting the waveguide is collimated in free-space and spectrally filtered with two dispersive prisms to remove the 1550 nm pump, 780 nm excitation, and frequency-doubled pump at 775 nm. Before detection with the Si SPADs, the light is further filtered using 20 nm bandpass filters centered at 710 nm. The experiments described in this manuscript used two different kinds of single-photon counting avalanche photodiodes (SPADs). The first kind (Perkin-Elmer [8]) has a quantum efficiency of ≈70 % near 710 nm and a timing jitter of ≈350 ps. The second kind (MPD [8]) has a quantum efficiency of ≈30 % near 710 nm and a timing jitter of ≈50 ps.

$g^{(2)}(0)$ determination

The extracted $g^{(2)}(0)$ values are determined by the $\tau = 0$ peak area and the average of the peak areas for $\tau \neq 0$. Errors in the extracted $g^{(2)}(0)$ values are determined by the propagation of errors due to shot noise in the $\tau = 0$ peak area and the standard deviation of the peak areas far from $\tau = 0$.

PULSED UPCONVERSION: EFFICIENCY

The efficiency of the pulsed upconversion process in a quasi-phase matched nonlinear medium can be calculated using the field evolution equations [9],

$$\frac{E_i}{dz} = \frac{i\omega_i d_Q}{n_i c} E_o E_p^* \exp(i\Delta k_Q z) \tag{1}$$

$$\frac{E_p}{dz} = \frac{i\omega_p d_Q}{n_p c} E_o E_i^* \exp(i\Delta k_Q z) \tag{2}$$

$$\frac{E_o}{dz} = \frac{i\omega_o d_Q}{n_o c} E_i E_p \exp(-i\Delta k_Q z) \tag{3}$$

where ω_i, ω_p, and ω_o are the input, pump, and output angular frequencies; n_i, n_p, and n_o are the indices of refraction of the input, pump, and output fields; d_Q is the effective non-linear coupling coefficient; E_i, E_p, and E_o are the input, pump, and output field amplitudes; z is the position along the crystal; and Δk_Q is the phase mis-match. In the limit where the pump is not depleted as it propagates through the crystal ($E_p \gg E_i, E_o$) and under phase-matching ($\Delta k_Q \approx 0$), these equations reduce to

$$\frac{E_i}{dz} = \frac{i\omega_i d_Q}{n_i c} E_o E_p^* \tag{4}$$

$$\frac{E_o}{dz} = \frac{i\omega_o d_Q}{n_o c} E_i E_p. \tag{5}$$

Solving these equations with initial condition $E_o(0) = 0$, yields

$$|E_o(L)|^2 = \frac{\omega_o}{\omega_i} |E_i(0)|^2 \sin^2\left(\sqrt{\frac{\omega_i \omega_o d_Q^2 L}{n_o n_i c^2}} |E_p|^2\right) \tag{6}$$

for the amplitude in the output field at the exit face of the non-linear crystal ($z = L$). This can be more conveniently expressed as

$$|A_o|^2 = \eta_{max} |A_i|^2 \sin^2\left(\alpha\sqrt{P}\right), \tag{7}$$

where $|A_o|^2 \propto |E_o(L)|^2/\omega_o$ and $|A_i|^2 \propto |E_i(0)|^2/\omega_i$ are the single photon field intensities (in units of photons), η_{max} is the maximum experimentally achievable conversion efficiency to account for non-idealities, $\alpha \propto \sqrt{\frac{\omega_i \omega_o d_Q^2 L}{n_o n_i c^2}}$, and P is the optical power of the pump beam. This expression can be extended straight-forwardly to time-dependent field amplitudes provided that the spectral bandwidth of the pulses are much narrower than the phase-matching bandwidth. For our PPLN waveguide, this bandwidth was measured to be ≈ 0.35 nm [4], corresponding to a pulse duration of ≈ 10 ps. All pulses in the experiment are at least an order of magnitude larger, validating the use of this expression. Since the field amplitudes are now time-dependent, the total efficiency can be expressed as

$$\eta_{tot} = \frac{\int dt |A_o(t)|^2}{\int dt |A_i(t)|^2}. \tag{8}$$

Defining $\int dt |A_i(t)|^2 = 1$, this becomes

$$\eta_{tot} = \eta_{max} \int dt |A_i(t)|^2 \sin^2\left(\alpha\sqrt{P(t)}\right). \tag{9}$$

For our experiment, $P(t)$ is a Gaussian pulse with a peak power corresponding to the maximum measured conversion efficiency using a CW beam. This power, P_{peak}, is 85 mW and corresponds to $\eta_{max} = 0.75$ [4]. Because P_{peak} was the roll-over point of the efficiency curve, we can therefore conclude that $\alpha P_{peak} = \pi/2$ and use $\eta_{max} = 0.75$ for subsequent calculations. We model the input photon as a exponentially-decaying wave-packet with time constant $\tau = 1.5$ ns. In total, the efficiency can be calculated as

$$\eta_{tot} = \frac{\eta_{max}}{\tau} \int_{-\infty}^{\infty} dt\, \Theta(t) e^{-t/\tau} \sin^2\left[\frac{\pi}{2} e^{-(t-\Delta T_{mod})^2/4\sigma^2}\right], \tag{10}$$

where $\Theta(t)$ is the Heaviside function, $\tau_{mod} = 2\sigma\sqrt{2ln2} \approx 2.35\sigma$ is the FWHM of the Gaussian pump pulse, and ΔT_{mod} is the delay between the pump pulse and the input single photon. Figure 4(c) of the main text was determined by maximizing Eq. 10 with respect to ΔT_{mod} as a function of τ_{mod}. An important experimental consequence of Eq. 10 is that the pump pulse is effectively broadened by the $\sin^2$ dependence of the efficiency. This broadening is displayed in Fig. 2. The FWHM of the effective pump pulse is ≈ 1.417 times larger than the FWHM of the Gaussian. This is the reason why the upconverted single photon using a pump pulse of $\tau_{mod} = 260$ ps was measured to have a FWHM of 350 ps when measured with the fast detector (timing jitter <50 ps) as shown in Fig. 3(c) of the primary manuscript. In fact, one calculates that the width should be 368 ps $\pm$ 22 ps, well within the uncertainty in the measurement.
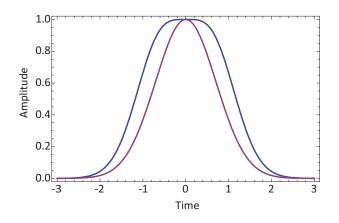
FIG. 2. Plot of a Gaussian with $\sigma = 1$ (maroon) as well as the $\sin^2$ of the square root of the same Gaussian (blue).

The fact that this estimate yields a value consistent with the measured FWHM gives further justification that this efficiency analysis is valid for our experiment.

The photon count rate is then the product of the total conversion efficiency η_{tot}, the photon collection efficiency η_{coll}, and the repetition rate of the 780 nm pulsed laser used to excite the QD. This relationship is valid provided each excitation pulse is sufficiently powerful so as to saturate the QD transition.

COMPLEX PULSE SHAPES

Aside from the simple Gaussian pump profiles used in the experiments detailed in the primary manuscript, it is possible to generate more complex pump pulses by creating more complex electrical pulses to drive the EOM. Figure 3 displays two examples of such pulses; an inverted Gaussian is displayed in (a) and a double pulse is displayed in (b). The level of complexity is only limited by the ability to generate the proper electrical pulse.
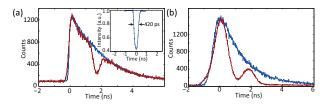

FIG. 3. (a) Temporal profile of upconverted photons using an inverted Gaussian pump (inset) with $\tau_{mod} = 420$ ps. (d) Temporal profile using a double-pulsed pump shape. All measurements are taken with 1200 s integration.

* matthew.rakher@gmail.com; Current Address: Departement Physik, Universität Basel, Klingelbergstrasse 82, CH-4056 Basel, Switzerland
[1] A. Stintz, G. T. Liu, H. Li, L. F. Lester, and K. J. Malloy, IEEE Photonics Tech. Lett. **12**, 591 (2000).
[2] K. Srinivasan, O. Painter, A. Stintz, and S. Krishna, Appl. Phys. Lett. **91**, 091102 (2007).
[3] J. C. Knight, G. Cheung, F. Jacques, and T. A. Birks, Opt. Lett. **22**, 1129 (1997).
[4] M. T. Rakher, L. Ma, O. Slattery, X. Tang, and K. Srinivasan, Nature Photonics **4**, 786 (2010).
[5] L. Ma, O. Slattery, and X. Tang, Opt. Express **17**, 14395 (2009).
[6] R. T. Thew, H. Zbinden, and N. Gisin, Appl. Phys. Lett. **93**, 071104 (2008).
[7] Q. Zhang, C. Langrock, M. M. Fejer, and Y. Yamamoto, Opt. Express **16**, 19557 (2008).
[8] Identified in this paper to foster understanding, without implying recommendation or endorsement by NIST.
[9] L. E. Myers, R. C. Eckardt, M. M. Fejer, R. L. Byer, W. R. Bosenberg, and J. W. Pierce, J. Opt. Soc. Am. B **12**, 2102 (1995).